J Nanopart Res (2020) 22: 251
https://doi.org/10.1007/s11051-020-04977-6

RESEARCH PAPER

Quantitative measurement of nanoparticle release from rubber composites during fabrication and testing

Louis Waquier · B. Steven Myles · Louis Henrard · Frederic Vautard · Christopher M. Pappas · Bruno Feneon · Caroline Delaitre · Jeremy J. Mehlem · Constantine Y. Khripin

Received: 6 March 2020 / Accepted: 5 August 2020 / Published online: 18 August 2020

Abstract Carbon black has been a key ingredient in high-performance composites, such as tire rubber, for over a hundred years. This reinforcing filler increases rubber rigidity and reduces tire wear, among many other useful effects. New nanomaterials, such as graphene and carbon nanotubes, may bring new performance improvements. However, their usefulness cannot be evaluated unless worker safety is assured by demonstrating that the nanoparticles are not released at harmful concentrations during manufacture and testing. Here, we present a flexible, general method for the quantitative evaluation of nanoparticle release from rubber nanocomposites. We evaluate manufacturing steps such as powder handling, uncured rubber milling, and curing. We also evaluate particle emission during cured rubber abrasion as an aggressive example of the testing rubber goods are subjected to. We quantify released nanoparticle concentrations for clay nanoparticles, graphene-like materials, and carbon nanotubes. We also describe a mechanistic framework based on the balance of adhesive and kinetic energies, which helps understand when nanoparticles are or are not released. This method contributes to the assessment of workers' exposure to nanoparticles during the various stages of the industrial process, which is an essential step in managing the risk associated with the use of nanomaterials in manufacturing.

Keywords Graphene · Carbon nanotube · Nanoparticle composite · Rubber · Environmental and health effects

Introduction

Fillers, such as silica and carbon black, have been used in rubber composites for decades (Donnet and Voet 1976; Vilgis et al. 2009) producing performance improvements such as reduced tire wear, reduced rolling resistance, and shorter vehicle braking distances. New nanomaterials, such as carbon nanotubes (CNTs) (Iijima 1991) and graphene (Novoselov et al. 2005), have the potential to become the next generation of rubber fillers, yet they have not found many commercial applications, in part due to unknown hazards which limit their industrial investigation.

Over the last few decades, we have made real progress in our knowledge of nanoparticle toxicology, especially of the mechanisms of action responsible for the toxicity of nanoparticles. Concepts that help us to better understand the risks associated with nanoparticles and nanofibers include the fate of particles in the body and the particle load that penetrates the body. As Mickael

Electronic supplementary material The online version of this article (https://doi.org/10.1007/s11051-020-04977-6) contains supplementary material, which is available to authorized users.

L. Waquier · B. S. Myles · L. Henrard · F. Vautard · C. M. Pappas · J. J. Mehlem · C. Y. Khripin (✉)
Michelin North America, 515 Michelin Rd., Greenville, SC 29605, USA
e-mail: constantine.khripin@michelin.com

B. Feneon · C. Delaitre
Manufacture Française des Pneumatiques Michelin, Place des Carmes Déchaux, 63040 Clermont-Ferrand Cedex 9, France

Riediker recently summarized (Riediker et al. 2019), toxicity depends on the "five Bs" of bioavailability, biopersistence, bioprocessing, biomodification, and bioclearance of nanoparticles. These factors in turn depend on key physical and chemical characteristics, such as particle shape, size (Chang et al. 2011; Xiong et al. 2011), and surface chemistry (Akhavan and Ghaderi 2010; Sasidharan et al. 2011; Wohlleben et al. 2016).

The complicated set of factors influencing nanoparticle toxicity make it difficult to predict. For example, amorphous silica nanoparticle toxicity depends on surface chemistry, with fumed silica being much more toxic than precipitated silica (Zhang et al. 2012). Titanium dioxide microparticles are considered safe, but nanoparticles are classified as a possible carcinogen (Skocaj et al. 2011). For this material, toxicity scales with surface area, meaning that the smaller the particle, the more toxic it is (Liao et al. 2009). Individually dispersed, straight carbon nanotubes are more toxic than tangled carbon nanotubes, perhaps because they do not fall under the fiber paradigm (Catalán et al. 2016). Thus, any commercial nanoparticle intended for a consumer product (or even simply evaluated in a research lab) must be treated as unique from the health and safety standpoint.

To assure the safety of workers carrying out the testing of rubber nanoparticle composites, the concentration of nanoparticles emitted during manufacturing and testing steps must be determined to be sufficiently below reasonable exposure limits (John Howard 2013; Lee et al. 2019). To date, there is no generally accepted method for doing so (Ding et al. 2017). Although there have been a number of academic studies of nanoparticle release under conditions typical of industrial manufacture, e.g., composite cutting and abrasion (Wohlleben et al. 2016; Cena and Peters 2011), there is not yet a simple, quantitative, and generally applicable method. In some cases, these studies have used complex equipment not generally available to the industry (Wohlleben et al. 2016). In other cases, there was no concentration quantification, or it was not specific to the nanoparticle of interest (Cena and Peters 2011; Bello et al. 2009; Schlagenhauf et al. 2012). Alternatively, the particle concentration was quantified, but the particles were not positively identified by microscopy (Lo et al. 2011). Thus, there is a need for the development of simple, quantitative methods to measure the release of nanoparticles during nanocomposite manufacture and testing.

We report a straightforward, quantitative, and relatively inexpensive method for measuring nanoparticle release from rubber composites. This method is applied to several types of rubber composites, measuring the release of various nanomaterials including clays, graphene-like materials, and carbon nanotubes. We test several manufacturing and rubber testing operations: powder handling, liquid dispersion decanting, external mixing (milling), rubbing solvent on uncured rubber, rubber curing, and the abrasion of cured rubber samples. The abrasion of cured samples was chosen due to its severity, and potential to release nanoparticles, to be a "severe scenario" for nanoparticle release during industrial rubber testing.

Materials and methods

The rubber fillers used were reduced graphene oxide (RGO, N002-PDR, Global Graphene Group), graphene nanoplatelets (GNP, grade 4124, Asbury Carbon), multi-wall CNTs (MWCNTs, Graphistrength®, Arkema, Inc.), single-wall CNTs (SWCNTs, TUBALL™, OCSiAl Inc.), kaolin clay (Polyfil® HG90, Kamin®, LLC), attapulgite clay (Actigel 208 palygorskite from Active Materials), molybdenum disulfide (Sigma-Aldrich), and precipitated silica (Zeosil 1165 MP, Solvay Inc.).

The following rubber mix components were obtained from standard rubber industry sources: styrene butadiene rubber (SBR, grades with $T_g = -65$ °C and -49 °C); treated distillate aromatic extract oil (TDAE); aliphatic resin ($T_g = 50$ °C), diphenyl guanidine (DPG); stearic acid, n-(1,3-dimethylbutyl)-n'-phenyl-p-phenylenediamine (6PPD); ZnO, bis(triethoxysilylpropyl)tetrasulfide (Si69®); n-octyltriethoxysilane (Octeo); and sulfur (S) and n-cyclohexyl-2-benzothiazole sulfenamide (CBS).

For release studies on nanomaterial types, two types of rubber compounds typical of tire treads were used: diluted and undiluted (Table 1). Unless noted otherwise, each mix had only one kind of filler. DPG and Si69 were used only in mixes containing attapulgite and silica.

The components were mixed in a 60 g scale Banbury mixer (Haake PolyLab OS Rheodrive 16, Thermo Fisher) for 5 min. The mixer temperature was set to 120 °C, and the rotor speed was 90 rpm. The mix was then passed 12 times through a 2-roll mill (Braebender® CWB Prep-Mill®) at 70 °C, with the addition of

curatives. The rubber mix was then cured at 150 °C, with the cure time determined from rheometric measurements.

A DIN abrader (Gibitre Instruments, ASTM D5963-04 (2010)) was used for the abrasion experiments. This instrument produces fine rubber particles without sample overheating or rubber smearing. A cylindrical sample 1.5 cm high and 1.6 cm in diameter is loaded (10 N) against a rotating drum with 60 grit corundum abrasive. The drum then begins to rotate with a tangential velocity of 0.3 m/s, and the sample is moved across the drum for a total sliding length of 40 m for one run (Fig. 1, see also Online Resource). The cylindrical sample is also rotated about its axis during translation to produce even abrasion.

The experiment was designed to detect any cross-contamination between samples. For each nanomaterial composite, data from 12 runs on the abrader were collected. After each nanomaterial run, e.g., of the RGO composite, 12 abrasion runs with a control silica rubber compound were performed to ensure that no RGO particles remained on the drum. The air was sampled, and collected particles were examined. This procedure was followed for all studies in this paper, and no cross-contamination was observed.

Table 1 Rubber mix formulations

Mix type	Undiluted*	Diluted*
Elastomer		
SBR T_g − 65 °C		100
SBR T_g − 49 °C	100	
Filler		
Silica, 160 m^2/g	45	
Kaolin, 22 m^2/g	105	
Attapulgite, 150 m^2/g	51	
SWCNT		12
MWCNT		30
RGO		16 or 20
GNP	30	
Additives		
DPG	1.8	
Stearic acid	1.2	
6PPD	2	
ZnO	2	
Oil, TDAE		12
Resin, Tg =50 °C		60
Si69	4.5	11
S	1.5	0.9
CBS	1.5	3.3

*Concentrations are given in units of per hundred rubber (phr)

Air sampling for nanoparticle collection is illustrated in Fig. 1 (see also Online Resource §2.A, especially Figs. S-4 and S-13). Briefly, air was aspirated from the point of abrasion using a sampling manifold with a rectangular intake 4 mm high and 20 mm wide located 1 cm from the sample being abraded. The air passed through approximately 1 m of 1/8" ID plastic tubing into the analysis instruments. For experiments other than abrasion, a similar setup was created to aspirate air from the point of potential nanoparticle generation, e.g., above mill rollers for rubber milling. The effect of the tubing was tested by measuring the ambient particle count with and without the tubing, and no difference was detected.

Two analysis instruments were used: Condensation Particle Counter (CPC, Model 3007 TSI Inc.) and Mini Particle Sampler (MPS, Ecomeasure Inc.) connected to a calibrated pump (GilAir Plus, Sensidyne Inc.). These are comparatively inexpensive, readily available instruments typically used for occupational safety monitoring.

Pump calibration was verified using the Gilibrator 2 air flow meter (Sensidyne Inc.) to be within 5% of specification. The calibration was not performed for each sample collection run but instead after the all the testing was completed. The CPC was used to determine the total count of particles. This information was used to ensure the background count was low and the system was working correctly. The MPS, with an air flow rate of 1000 cc/min ± 5%, was used to collect particles on holey carbon TEM grids (R1.2/1.3400 Cu mesh, Quantifoil Inc.). Pressure drop across the MPS grid was monitored to ensure there were no leaks (e.g., see Online Resource §2.B). The CPC was used qualitatively only, while the MPS was used to identify and quantify the concentration of nanoparticles.

The efficiency of particle collection for the Quantifoil carbon grids has previously been reported for spherical particles (R'mili et al. 2013). To calculate efficiency for non-spherical particles, we use intrinsic viscosity and Stokes number calculations to obtain the efficiency, see Online Resource §1 for details. Efficiency ranges from 1 for the larger RGO particles to 0.1 for SWCNTs.

The grids were imaged on a Scanning Transmission Electron Microscope (STEM, JEOL JSM-7100F) in TEM mode. The airborne concentration of nanoparticles

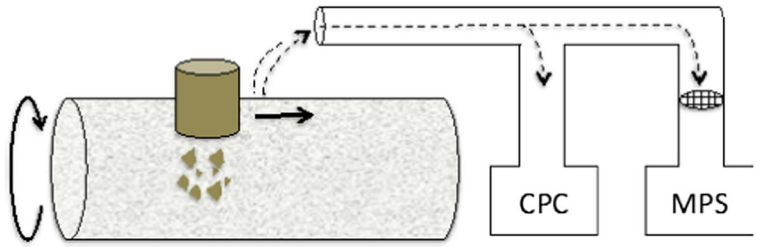

Fig. 1 Experimental abrasion setup. A rubber sample is abraded on a sandpaper drum, while the air is collected and analyzed

was quantified as follows (for details see Online Resource §2.D). First, images were collected in an X pattern across the grid to calculate a quantitative concentration of the particles on the grid. Between 10 and 40, 10 × 10 or 20 × 20 μm images were collected per grid depending on the desired accuracy, particle concentration, and particle size. Considering that the laminar flow in the MPS is not isokinetic, we expected that particles may not be evenly distributed on the TEM grid and therefore collected a large number of images in a consistent pattern across the grid. Second, the types of nanoparticles present in the images were catalogued. Finally, air flowrate, collection efficiency, and a geometric estimate of the particle mass were used to calculate the mass concentration of each nanoparticle type.

Care was taken to consider possible false positives from ambient nanoparticles. Using a separate MPS instrument, nanoparticles from ambient air were collected during the abrasion tests at a location near the tester to ensure that the particles being quantified were not present naturally. Please see Online Resource §2.D for examples of naturally occurring nanoparticles. If ambient particles were similar to test particles, or ambient CPC concentration was high, the abrasion tester was operated under HEPA filtered air (SS-200-MSP, Sentry Air Systems Inc., Houston, TX) such that the concentration of ambient nanoparticles detected by the CPC was < 10 per cc.

Results and discussion

Rates of nanoparticle release from composites are generally low. For example, several studies of CNT composites have been carried out, and in most cases, no CNT release was detected (Cena and Peters 2011; Bello et al. 2009; Schlagenhauf et al. 2012). We explain the rarity of released nanoparticles by considering the balance of kinetic and adhesive forces during the most likely nanoparticle release route: kinetic energy transfer to a loose particle on the rubber surface. To our knowledge, no other compelling mechanism for nanoparticle release from rubber composites has been proposed. Loose nanoparticles could be generated during the process of abrasion, which would expose them on the surface and displace them laterally along the surface. Alternatively, loose particles may arise due to inclusions of undispersed particles in the composite. In order to determine the likelihood of such a loose particle being released, we calculate conservative, low-end estimates for their adhesion energy and compare it to the kinetic energy which could come from an abrading asperity.

To estimate the adhesion energy, we use the Derjaguin approximation, which is a point-wise integration over the objects in contact. This approximation is valid for cases where the contact is much smaller than the objects, which is true in our case. We consider idealized particle shapes—spheres, rods, and plates—to take advantage of well-established mathematical formulations. Adhesion energy due to Van der Waals (VdW) forces for a sphere resting on a half-space, E_{ad}, is given by (Israelachvili 2011):

$$E_{\mathrm{ad}} = \frac{AD}{6d} \tag{1}$$

where A is the Hamaker constant, 5E-20 J for hydrocarbons, D is the sphere diameter, and d is the distance between the sphere and surface, assumed to be 0.2 nm for close contact. For a rod in contact with a half-space, this becomes (Israelachvili 2011):

$$E_{\mathrm{ad}} = \frac{ALD^{0.5}}{24\sqrt{d^3}} \tag{2}$$

where L is the length of the rod, taken as 100D for demonstrative purposes. For a flat plate, such as a kaolin flake, or several-layer graphene, in contact with a half-space, the adhesion energy is (Israelachvili 2011):

$$E_{\mathrm{ad}} = \frac{ALW}{12\pi d^2} \tag{3}$$

These are conservative values for particles which are resting on the surface; if they were enveloped in the material (or the contact is compliant), the energies would be higher (Carrillo et al. 2010; Kendall et al. 2011; Cao et al. 2014).

The adhesion energies for spheres, rods, and plates are plotted in Fig. 2. In addition to VdW forces, covalent bonds can increase the restraining energy. Taking a generic value of 350 kJ/mol for the breaking energy of a single covalent bond, we plot the energy for a single bond restraining the particle. The energy of a single covalent bond is lower than the adhesive energies; however, if there are multiple covalent bonds, the situation will be different. For example, if a plate-like particle was covalently bonded to the surface with a bond density of 0.059 bonds/nm^2, the covalent bond energy would be greater.

For comparison, we also plot reported experimentally measured adhesion energies for SWCNTs (Buchoux et al. 2011), MWCNTs (Ishikawa et al. 2009), graphene (Jiang and Zhu 2015), soot (spherical nanoparticles) (Liu et al. 2018), and PVC microspheres (Zimon 1969) on various substrates. The measured adhesion energies are uniformly higher than our estimated energies. Our estimate is based on conservative assumptions and could serve as a lower bound. For example, the Hamaker constant has been reported to be up to 10 times higher for soot particles (Liu et al. 2018). In addition, particle deformation due to adhesive forces may increase the area of contact, and forces other than VdW, such as electrostatic, hydrogen bonding, etc., may play a role (Liu et al. 2018; Zimon 1969).

We now move to obtaining an estimate for "releasing" forces. To leave the surface, the particle must have sufficient energy, thermal or kinetic. Kinetic energy is given by:

$$E_{\mathrm{k}} = \frac{1}{2}\rho V v^2 \tag{4}$$

where ρ is the particle density, 2 g/cm^3, V is the particle volume, and v is the velocity of the particle, assumed to be the same as the abrading surface asperity, depending on experimental conditions, 2 m/s (Wohlleben et al. 2016), for example. Alternatively, the impetus may come from thermal energy, approximately equal to $k_{\mathrm{b}}T$. We plot this for 300 K in Fig. 2.

To evaluate the likelihood of particle release, we compare the energy values in Fig. 2. First, both the kinetic and adhesive energies are much larger than

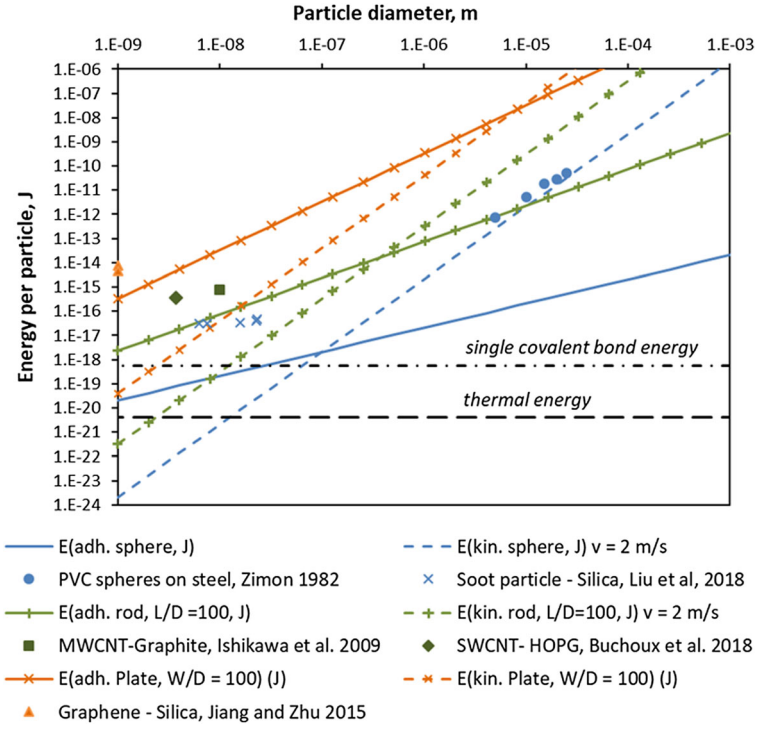

Fig. 2 The kinetic and adhesive energies for rods, spheres, and plates are given as a function of diameter (or thickness for plates). The point of release, where kinetic energy exceeds adhesive energy, occurs where the lines intersect. Thermal energy, $k_{\mathrm{b}}T$, and the rupture energy of a covalent bond are shown for comparison

thermal energy, which can be neglected. This implies that nanoparticles cannot diffuse away from the surface without additional kinetic energy. For spheres, the kinetic energy exceeds the adhesive energy at a diameter of ~ 100 nm; for rods, this is even larger, occurring at a diameter of ~ 1 μm. Of course, restraining and releasing energies would have a distribution of values, so some particles may be released; however, this argument explains why release is rarely observed for nanoparticles.

Industrial development of nanocomposites involves many destructive tests, for example, pull to break, crack propagation, and abrasion. Of these, abrasion can be viewed as a worst-case scenario due to the large amount of liberated surface area from which release may occur. Thus, we consider abrasion, Fig. 1, to be a good candidate for a nanoparticle release test to evaluate the safety of nanocomposites in the manufacturing environment. The DIN abrader abrades rubber through the crack growth mechanism, as opposed to through fatigue smearing which occurs on less abrasive surfaces (Schallamach 1968). Rubber abraded through fatigue smearing is very soft and adhesive and traps particles from the environment rather than releasing them (Camatini et al. 2001; Adachi and Tainosho 2004).

We have selected the ASTM abrasion method for its simplicity, general availability, and lack of rubber smearing. Our approach differs from a previously reported test on nanoparticle release from rubber in having a lower sample velocity, 0.3 m/s vs 1.8 m/s, but higher pressure, 0.5 bar vs 1.6 bar, resulting in smaller energy input, 15 kW/m^2 vs 29 kW/m^2 (Wohlleben et al. 2016). Studies on hard plastic materials have employed similar to somewhat higher energy inputs. A study on epoxy composites used manual sanding to generate dust (Cena and Peters 2011). Another study on epoxy-CNT composites employed a band saw and a cutting wheel with speeds of 20 m/s and 15 m/s, respectively (Bello et al. 2009). A third study utilized a Taber abrader at 60 Hz, corresponding to a linear speed of approximately 0.3 m/s. Thus, the intensity of our abrasion method is somewhere in the middle of reported methods.

Rubber reinforced with reduced graphene oxide (RGO) has been investigated by many groups (Hernández et al. 2012; Young et al. 2012) and therefore serves as a good subject for testing the release of nanoparticles from industrial composites. We tested several rubber formulations reinforced with RGO, Table 2, see also Online Resource §2, to investigate the effect of RGO concentration and of adding a second filler type, silica. The CPC detector registered higher particle counts for RGO than for the silica witness. The particles counted by the CPC were largely not RGO, since the number concentration of RGO platelets calculated from TEM observation was only ~ 0.1 per cc, negligible compared with the CPC count. It is not clear what caused the high CPC count; presumably, it is molecular clusters small enough to trigger condensation but too small for TEM detection on the grid.

RGO sheets (Fig. 3h) were observed on the MPS grids from several of the samples. The calculated concentrations, 4–13 ng/m^3, Table 2, were near the detection limit, 1 ng/m^3, which would correspond to a single flake observed in 40 10 × 10 μm images. It would have been preferable to use larger TEM images to detect more particles. However, since these concentrations are several orders of magnitude below proposed exposure limits (Lee et al. 2019), this accuracy is sufficient. The ± indicates 95% interval for standard error in the mean. Various types of ambient nanoparticles were also detected on the MPS grids. Smoke, clay, etc. were catalogued (see Online Resource §2.D.a). The concentration of these nanoparticles was < 0.1 μg/m^3. The distinctive nature of RGO made identification of the target nanoparticle among ambient particles unambiguous.

An industrial method for quantifying the release of nanoparticles should be able to function with a variety of particle types and serve as a "worst-case scenario"

Table 2 Airborne concentrations of nanoparticles measured during abrasion of RGO materials

Sample	Mix description	CPC mean #/cc	Ambient nanoparticles,* μg/m^3	RGO, μg/m^3
SiO2	110 phr silica	1700 ± 400	0.088	0
RGO 1	8 phr RGO	14,000 ± 4000	0.005	4E-3 ± 8E-3
RGO 2	10 phr RGO	50,000 ± 14,000	0.014	0.013 ± 8E-3
RGO 3	4 phr RGO, 55 phr silica	9000 ± 3000	0.034	0.007 ± 8E-3

*The concentration of ambient nanoparticles varied day to day, and averages are given for 6 SiO_2 samples and 2 of each RGO sample

release benchmark. We applied this method to detect various types of nanoparticles released from rubber during abrasion. Sample SEM images of the particles as captured on TEM grids are shown in Fig. 3. The MWCNT agglomerates and single MWCNTs are very close in appearance to those reported in previous studies of nanoparticle release (Wohlleben et al. 2016; Schlagenhauf et al. 2012). Others, such as RGO, GNP, and nanoclays, have not yet been reported. In addition to these novel nanomaterials, we examined commonly used rubber fillers: silica, alumina, molybdenum disulfide, and kaolin clay and found that only kaolin compounds released nanoparticles (Online Resource §4).

Concentrations of released nanoparticles were quantified for a range of nanoparticle types (Fig. 4). In general, larger concentrations are observed for larger particles, as predicted (Fig. 2). We consider the detection limit as being able to observe a single particle in a reasonable SEM survey of the MPS grid, for example, 40 distributed images. Release limits in Fig. 4 were obtained from the following sources: OSHA (29 CFR §1910.1000) for attapulgite clay, NIOSH guidelines for CNTs, and Lee et al. (Lee et al. 2019) for the graphene-like materials.

To measure particle release during uncured rubber processing steps, the CPC/MPS instruments were mounted on the equipment on which various operations were performed, sampling released nanoparticles in ambient air. Two mixes were used in the trials: an undiluted attapulgite mix and a diluted RGO mix (Table 1). During uncured rubber milling (see also Online Resource §3), the attapulgite mix showed no particle release on the CPC instrument or on the MPS grids. The RGO mix did show some particles on the CPC counter; however, MPS analysis showed that these were amorphous uncured rubber particles, with no individual nanoparticles detected (Fig. 5, left). Further tests on the milling of uncured rubber, for example, rubber cutting and solvent application, did not produce any nanoparticle release.

The mechanism for nanoparticle release from uncured rubber may be different from that for cured rubber. As discussed above, uncured rubber is very sticky, and intuitively, we would not expect to observe released nanoparticles. Indeed, instead of adhesive energy for loose particles, plotted in Fig. 2, we would have adhesion energy for enveloped particles, which would be orders of magnitude higher (Cao et al. 2014). An alternate release pathway would be through liquid aerosolization (R'mili et al. 2013; Stern et al. 1974). As airborne droplets evaporate, suspended nanoparticles would remain airborne. However, since rubber cannot evaporate, such aerosols would not release free nanoparticles. Thus, we cannot propose any reasonable pathway for release of nanoparticles from green rubber.

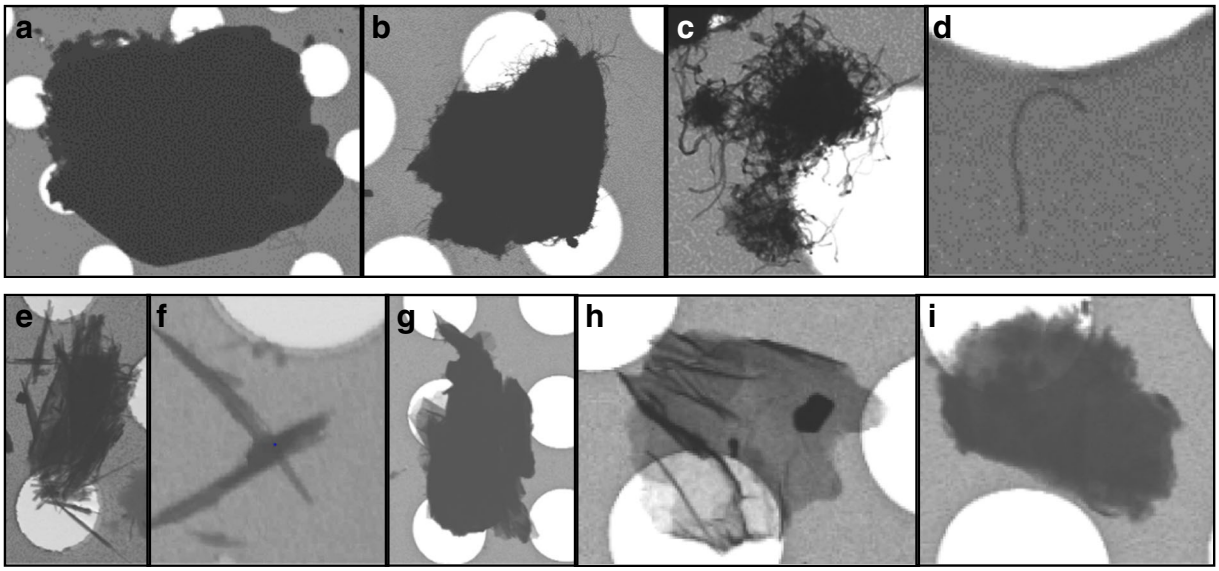

Fig. 3 Particles captured on TEM grids during rubber abrasion: **a**, rubber particle; **b**, rubber particle with protruding MWCNT; **c**, undispersed MWCNT agglomerate; **d**, isolated MWCNT; **e**, clay agglomerate; **f**, clay particle; **g**, rubber particle with protruding RGO; **h**, isolated RGO; **i**, isolated GNP. The hole diameter is 1.5 μm

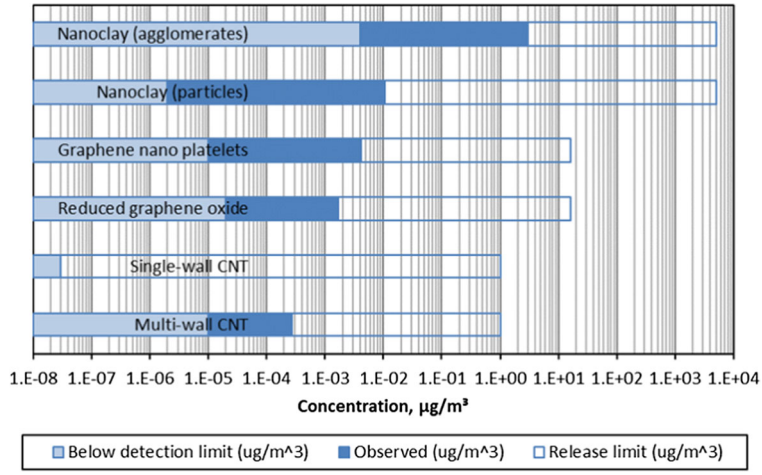

Fig. 4 Concentration of various nanoparticles released from rubber during abrasion

Nanomaterial powders are often incorporated into rubber on 2-roll mills, see, for example (Hernández et al. 2012). We carried out several tests to examine whether this process step produced airborne nanoparticles (see also Online Resource §3.C, D). Two grams of attapulgite powder, placed on top of the milling rubber, resulted in an airborne concentration of 63 ± 6 µg/m^3 for micron-scale clay agglomerates (Fig. 3e) and 0.1 ± 0.02 ng/m^3 for nano-scale clay particles (Fig. 3f). One gram of RGO added on the mill resulted in 45 ± 8 µg/m^3 RGO agglomerates (Fig. 5, right) and 4 ± 1 ng/m^3 isolated sheets. Thus, it is possible for nanoparticles to be released during powder incorporation into uncured rubber.

Another test in which nanoparticle release was observed was the pouring of liquids. Decanting 100 cc of 0.5 wt% RGO solution (see Online Resource §3.F) produced emissions of 5 ± 2 ng/m^3. This can be explained by the aerosol droplet evaporation route (Stern et al. 1974).

Curing of rubber occurs at high temperatures (130–170 °C) and pressures (> 10 bar). Therefore, it is conceivable that volatile components may be emitted. CPC and MPS air sampling during the curing of a 150 g sample of 10 wt% RGO mix showed emission of amorphous droplets, possibly degraded polymer, oil (see Online Resource §3.G), or other high boiling point components, but no RGO nanoparticles were observed.

Conclusions

By combining a simple particle concentration measurement instrument, the CPC, with a particle identification and quantification instrument, the MPS, we have created a straightforward method for evaluating airborne concentrations of nanoparticles in realistic process conditions. This method can be applied to the study of particle emissions from a variety of nanoparticle-rubber composites. Our results show that at least for nanoclays, carbon nanotubes, and graphene-like materials, the airborne concentrations can be quantified at levels far below exposure limits, suggesting that this method can

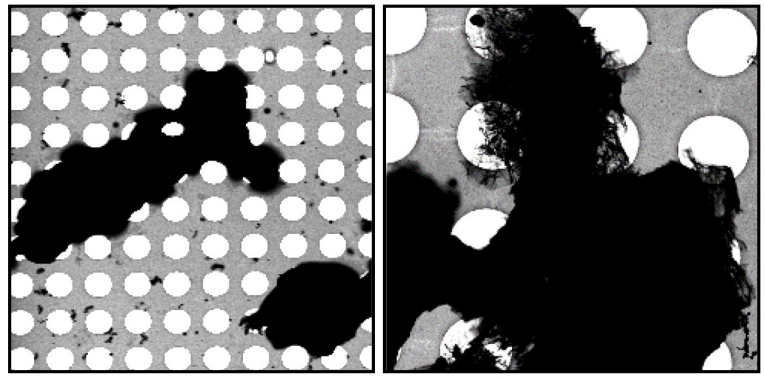

Fig. 5 (Left) Amorphous uncured rubber particles released during milling and (right) graphene particles released during powder processing

be used even under difficult conditions, for example, at high ambient particle counts, to assure worker safety. Concentrations of nanoparticles released are generally low, which is in accordance with previous results showing that nanoparticles generally flocculate. We explain this by showing that restraining adhesive forces are generally greater than releasing kinetic forces. These advances may facilitate safer development of novel nanocomposites.

Acknowledgments The authors are grateful to Dr. Olivier Le Bihan of the INERIS for the helpful discussions on the MPS method.

Funding information This work is wholly funded by the Michelin North America Inc., a subsidiary of the Compagnie Générale des Établissements Michelin, a global tire and rubber goods manufacturer.Data availabilityThe results presented in this paper are not proprietary, and data is available upon request.

Compliance with ethical standards

Conflict of interest The authors are or were employees of the Michelin North America Inc., a subsidiary of Compagnie Générale des Établissements Michelin, a global tire and rubber goods manufacturer.

References

Adachi K, Tainosho Y (2004) Characterization of heavy metal particles embedded in tire dust. Environ Int 30:1009–1017

Akhavan O, Ghaderi E (2010) Toxicity of graphene and graphene oxide nanowalls against bacteria. ACS Nano 4:5731–5736

Bello D, Wardle BL, Yamamoto N, Guzman DeVilloria R, Garcia EJ, Hart AJ, Ahn K, Ellenbecker MJ, Hallock M (2009) Exposure to nanoscale particles and fibers during machining of hybrid advanced composites containing carbon nanotubes. J Nanopart Res 11:231–249

Buchoux J, Bellon L, Marsaudon S, Aimé J-P (2011) Carbon nanotubes adhesion and nanomechanical behavior from peeling force spectroscopy. Eur Phys J B 84(1):69–77

Camatini M, Crosta GF, Dolukhanyan T, Sung C, Giuliani G, Corbetta GM, Cencetti S, Regazzoni C (2001) Microcharacterization and identification of tire debris in heterogeneous laboratory and environmental specimens. Mater Charact 46:271–283

Cao Z, Stevens MJ, Dobrynin AV (2014) Adhesion and wetting of nanoparticles on soft surfaces. Macromolecules 47:3203–3209

Carrillo J-MY, Raphael E, Dobrynin AV (2010) Adhesion of nanoparticles. Langmuir 26:12973–12979

Catalán J, Siivola KM, Nymark P, Lindberg H, Suhonen S, Järventaus H, Koivisto AJ, Moreno C, Vanhala E, Wolff H (2016) In vitro and in vivo genotoxic effects of straight versus tangled multi-walled carbon nanotubes. Nanotoxicology 10(6):794–806

Cena LG, Peters TM (2011) Characterization and control of airborne particles emitted during production of epoxy/carbon nanotube nanocomposites. J Occup Environ Hyg 8:86–92

Chang Y, Yang S-T, Liu J-H, Dong E, Wang Y, Cao A, Liu Y, Wang H (2011) In vitro toxicity evaluation of graphene oxide on A549 cells. Toxicol Lett 200:201–210

Ding Y, Kuhlbusch TAJ, Van Tongeren M, Jiménez AS, Tuinman I, Chen R, Alvarez IL, Mikolajczyk U, Nickel C, Meyer J et al (2017) Airborne engineered nanomaterials in the workplace—a review of release and worker exposure during nanomaterial production and handling processes. J Hazard Mater 322:17–28

Donnet J-B, Voet A (1976) Carbon black: physics, chemistry, and elastomer reinforcement

Hernández M, del Mar Bernal MI, Verdejo R, Ezquerra TA, López-Manchado MA (2012) Overall performance of natural rubber/graphene nanocomposites. Compos Sci Technol 73:40–46

Iijima S (1991) Helical microtubules of graphitic carbon. Nature 354:56–58

Ishikawa M, Harada R, Sasaki N, Miura K (2009) Adhesion and peeling forces of carbon nanotubes on a substrate. Phys Rev B 80(19):193406

Israelachvili JN (2011) Intermolecular and surface forces

Jiang T, Zhu Y (2015) Measuring graphene adhesion using atomic force microscopy with a microsphere tip. Nanoscale 7(24):10760–10766

John Howard MD (2013) Occupational exposure to carbon nanotubes and nanofibers - CDC

Kendall K, Kendall M, Rehfeldt F (2011) Adhesion of cells, viruses and nanoparticles. Springer, New York

Lee Y-S, Sung J-H, Song K-S, Kim J-K, Choi B-S, Yu I-J, Park J-D (2019) Derivation of occupational exposure limits for multi-walled carbon nanotubes and graphene using subchronic inhalation toxicity data and a multi-path particle dosimetry model. Toxicol Res 8(4):580–586

Liao C-M, Chiang Y-H, Chio C-P (2009) Assessing the airborne titanium dioxide nanoparticle-related exposure hazard at workplace. J Hazard Mater 162(1):57–65

Liu Y, Song C, Lv G, Chen N, Zhou H, Jing X (2018) Determination of the attractive force, adhesive force,

adhesion energy and Hamaker constant of soot particles generated from a premixed methane/oxygen flame by AFM. Appl Surf Sci 433:450–457

Lo L-M, Hammond D, Bartholomew I, Almaguer D, Heitbrink W, Topmiller J (2011) Engineering controls for nano-scale graphene platelets during manufacturing and handling processes. National Institute for Occupational Safety and Health (NIOSH)

Novoselov KS, Jiang D, Schedin F, Booth TJ, Khotkevich VV, Morozov SV, Geim AK (2005) Two-dimensional atomic crystals. Proc Natl Acad Sci 102:10451–10453

R'mili B, Le Bihan OLC, Dutouquet C, Aguerre-Charriol O, Frejafon E (2013) Particle sampling by TEM grid filtration. Aerosol Sci Technol 47:767–775

Riediker M, Zink D, Kreyling W, Oberdörster G, Elder A, Graham U, Lynch I, Duschl A, Ichihara G, Ichihara S (2019) Particle toxicology and health-where are we? Part Fibre Toxicol 16(1):19

Sasidharan A, Panchakarla LS, Chandran P, Menon D, Nair S, Rao CNR, Koyakutty M (2011) Differential nano-bio interactions and toxicity effects of pristine versus functionalized graphene. Nanoscale 3:2461–2464

Schallamach A (1968) Abrasion, fatigue, and smearing of rubber. J Appl Polym Sci 12:281–293

Schlagenhauf L, Chu BTT, Buha J, Nüesch F, Wang J (2012) Release of carbon nanotubes from an epoxy-based nanocomposite during an abrasion process. Environ Sci Technol 46: 7366–7372

Skocaj M, Filipic M, Petkovic J, Novak S (2011) Titanium dioxide in our everyday life; is it safe? Radiol Oncol 45(4):227–247

Stern EL, Johnson JW, Vesley D, Halbert MM, Williams LE, Blume P (1974) Aerosol production associated with clinical laboratory procedures. Am J Clin Pathol 62:591–600

Vilgis TA, Heinrich G, Klüppel M (2009) Reinforcement of polymer nano-composites: theory, experiments and applications

Wohlleben W, Meyer J, Muller J, Müller P, Vilsmeier K, Stahlmecke B, Kuhlbusch TAJ (2016) Release from nanomaterials during their use phase: combined mechanical and chemical stresses applied to simple and multi-filler nanocomposites mimicking wear of nano-reinforced tires. Environ Sci Nano 3:1036–1051

Xiong D, Fang T, Yu L, Sima X, Zhu W (2011) Effects of nano-scale TiO2, ZnO and their bulk counterparts on zebrafish: acute toxicity, oxidative stress and oxidative damage. Sci Total Environ 409:1444–1452

Young RJ, Kinloch IA, Gong L, Novoselov KS (2012) The mechanics of graphene nanocomposites: a review. Compos Sci Technol 72:1459–1476

Zhang H, Dunphy DR, Jiang X, Meng H, Sun B, Tarn D, Xue M, Wang X, Lin S, Ji Z (2012) Processing pathway dependence of amorphous silica nanoparticle toxicity: colloidal vs pyrolytic. J Am Chem Soc 134(38):15790–15804

Zimon AD (1969) Adhesion of dust and powder (trans: corn M). Springer Science & Business Media, London